Turbulence, Heat and Mass Transfer 10

Assessment of LES models for a fully developed wind-turbine array boundary layer

D.Folch, F.X.Trias, A.Oliva
Heat and Mass Transfer Technological Center, Technical University of Catalonia
C/Colom 11, 08222 Terrassa (Barcelona)
http://www.cttc.upc.edu/
david.folch@upc.edu francesc.xavier.trias@upc.edu asensio.oliva@upc.edu

Abstract – Direct numerical simulations of the incompressible Navier-Stokes equations at high Reynolds numbers are not yet feasible, so dynamically less complex mathematical formulations such as Large Eddy Simulation (LES) have been developed. For the well-known eddy-viscosity models for LES, the computational method is based on the combination of invariants of a symmetric tensor that depends on the gradient of the resolved velocity field, $\mathsf{G} = \nabla\overline{u}$. Several models (namely S3PQR) have been developed using the first three principal invariants of the symmetric tensor $\mathsf{G}\mathsf{G}^T$ with excellent results. Therefore, in this work, we will focus on the application of the S3PQR and other LES models on the free boundary layer case. Then, we will test their performances over a fully developed boundary layer wind farm, using a simplified model of a wind turbine.

1. Introduction

The most useful tool to deal with turbulent flow is the incompressible Navier Stokes formulation. However, for large Reynolds numbers, that is, when it exists many relevant scales of motion of the flow, the direct numerical simulation is unfeasible or a very highly demanding resources procedure. To try and solve the problem, a number of mathematical methods have been created. However, if they are to be effective in addressing specific challenges, it is necessary to discriminate between them. The Large Eddy Simulation LES equations are derived from the application of a spatial filter to the incompressible Navier Stokes equations:

$$\begin{aligned} \partial_t\overline{u} + C(\overline{u},\overline{u}) &= D(\overline{u}) - \nabla p - \nabla\cdot\tau(\overline{u}); \\ \nabla\cdot\overline{u} &= 0 \end{aligned} \tag{1}$$

where $\overline{u}$ is the filtered velocity and $\tau(\overline{u})$ is the subgrid stress (SGS) tensor that approximates the effect of the under-resolved scales.

This equation needs a closure model to be numerically solved. The LES closure is of the type $\tau(\overline{u}) \approx -2\nu_e S(\overline{u})$ where $S(\overline{u}) = 1/2(\nabla\overline{u} + \nabla\overline{u}^T)$ is the rate-of-strain tensor. We must define an eddy viscosity: $\nu_e = (C_m\Delta)^2 D_m(\overline{u})$ where C_m is the model constant, Δ is the subgrid characteristic length, and $D_m(\overline{u})$ is the differential operator with units of frequency associated with the model [1].

As Menevau and Katz[2] point out, most successful tests typically use spectral methods and cutoff filtering on homogeneous directions. Our approach, then, is that of a pseudo-spectral algorithm.

To assure the validity of any of the models, usually, they are tested on what are called benchmark cases and compared with experimental results. These cases are, for example, the channel flow, the sink flow, the homogeneous isotropic turbulence, the boundary layer, and so on.

Besides, there are some technical specifications of the algorithm that could yield different performances of the model. That is, for example, the time-stepping procedure, the characteristic of the domain, or the mathematical approximations.

2. Review of S3PQR Theory

Besides the trace, several mathematical invariants can be calculated from the gradient tensor $\mathsf{G} = \nabla\overline{u}$, namely:

$$\{Q_{\mathsf{G}}, R_{\mathsf{G}}, Q_{\mathsf{S}}, R_{\mathsf{S}}, V_{\mathsf{G}}^2\}$$

For this second-order tensor G, they are defined as [3]

$$\begin{aligned} Q_{\mathsf{G}} &= (1/2)(tr^2(\mathsf{G}) - tr(\mathsf{G}^2)) \\ R_{\mathsf{G}} &= det(\mathsf{G}) \\ Q_{\mathsf{S}} &= (1/2)(tr^2(\mathsf{S}) - tr(\mathsf{S}^2)) \\ R_{\mathsf{S}} &= det(\mathsf{S}) \\ V_{\mathsf{G}}^2 &= 4(tr(S^2\Omega^2) - 2Q_S Q_\Omega) \end{aligned} \tag{2}$$

where $\mathsf{S} = 1/2(\mathsf{G} + \mathsf{G}^T)$ and $\Omega = 1/2(\mathsf{G} - \mathsf{G}^T)$ are the symmetric and the skew-symmetric parts of the gradient tensor, respectively. For any incompressible flux, any invariant can be written as a function of them

Most of the models of the LES algorithms are based on combinations of invariants [1] of some tensor depending on the gradient of the velocity. For example, they are the Smagorinsky model [4], Vreman's [5], WALE [6], or the S3PQR models [3]:

- Smagorinsky[4] model $\nu_e^{Smag} = f(Q_{\mathsf{S}})$
- Verstappen's[7] model $\nu_e^{Ve} = f(R_{\mathsf{S}}, Q_{\mathsf{S}})$
- WALE model[6] $\nu_e^{W} = f(Q_{\mathsf{G}}, V, Q_{\mathsf{S}})$
- Vreman's model[5] $\nu_e^{Vr} = f(V, Q_{\mathsf{G}}, Q_\Omega, Q_{\mathsf{S}})$
- σ-model[1] $\nu_e^{\sigma} = f(\lambda_1, \lambda_2, \lambda_3)$ where $\lambda_1, \lambda_2, \lambda_3$ are the $\mathsf{G}\mathsf{G}^T$ tensor eigenvalues

The S3PQR models[3] involve three invariants of the symmetric tensor $\mathsf{G}\mathsf{G}^T$ formally based on the lowest-order approximation of the subgrid stress tensor[8],

$$\tau(\overline{u}) = \frac{\Delta^2}{12}\mathsf{G}\mathsf{G}^T + \mathscr{O}(\Delta^4) \tag{3}$$

These invariants are directly related to the previous ones

$$\begin{aligned} P_{\mathsf{G}\mathsf{G}^T} &= tr(\mathsf{G}\mathsf{G}^T) = 2(Q_\Omega - Q_{\mathsf{S}}) \\ Q_{\mathsf{G}\mathsf{G}^T} &= 2(Q_\Omega - Q_{\mathsf{S}})^2 - Q_{\mathsf{G}}^2 + 4tr(\mathsf{S}^2\Omega^2) \\ R_{\mathsf{G}\mathsf{G}^T} &= det(\mathsf{G}\mathsf{G}^T) = det(\mathsf{G})det(\mathsf{G}^T) = R_{\mathsf{G}}^2 \end{aligned} \tag{4}$$

So now one can construct new models[3] of the form $\nu_e = (C_{s3pqr}\Delta)^2 P_{\mathsf{G}\mathsf{G}^T}^p Q_{\mathsf{G}\mathsf{G}^T}^q R_{\mathsf{G}\mathsf{G}^T}^r$
If we restrict them to solutions involving only two invariants, then we define:

$$\nu_e^{S3PQ} = (C_{s3pq}\Delta)^2 P_{\mathsf{GG}^T}^{-5/2} Q_{\mathsf{GG}^T}^{3/2} \quad (5)$$

$$\nu_e^{S3PR} = (C_{s3pr}\Delta)^2 P_{\mathsf{GG}^T}^{-1} R_{\mathsf{GG}^T}^{1/2} \quad (6)$$

$$\nu_e^{S3QR} = (C_{s3qr}\Delta)^2 Q_{\mathsf{GG}^T}^{-1} R_{\mathsf{GG}^T}^{5/6} \quad (7)$$

An important property of each of the S3PQR model is its 2D behaviour[1, 3]: only R_{GG^T}-dependent models switch off for 2D flows, so S3PR and S3QR models are preferable in this case.

Further characteristics of these LES models are positiveness, locality, Galilean invariance, and proper near-wall behaviour[9] ($\mathscr{O}(y^3)$ dependence on normal direction).

2.1 Test cases

Finally, there are two ways to determine the model constant for the S3PQR models:

1. Imposing numerical stability and less or equal dissipation than Vreman's model. Then,

$$C_{s3pq} = C_{s3pr} = C_{s3qr} = \sqrt{3}C_{Vr} \approx 0.458$$

2. Granting that the averaged dissipation of the models is equal to that of the Smagorinsky model. Then,

$$C_{s3pq} = 0.572,\ C_{s3pr} = 0.709,\ C_{s3qr} = 0.762$$

Therefore, we will call six possible combinations to test (3 model types x 2 constants) PQ1, PQ2, and so on. Added to them, we will also run the no-model algorithm, Smagorinsky's, Vreman's, and WALE ones.

In some cases, there have already been found differences in the numerical results depending on the constant chosen. For example, simulations of decaying isotropic turbulence have shown that only the last values provide the right SGS dissipation[3].

We will test the zero mean pressure gradient case.

3. Pseudo-spectral Algorithms

Pseudo-spectral methods have been shown to provide a high level of resolution for derivatives, and are seen as an excellent tool where periodic conditions[10] can be applied. These algorithms, however, require a strict presence of periodicity. But one of the main features of the boundary layer case is that it continually develops over the streamwise direction, so it is in no way periodic.

It is necessary then to use a different approach like the method proposed by Spalart[11, 12], which includes normal coordinate similarity transformations, growing terms $GT(\overline{u},\overline{U})$, and several other assumptions. Since our objective is to check whether the S3PQR models can be adapted to the special characteristics of the boundary layer in a pseudo-spectral manner, we will not discuss further the validity of the periodic configuration.

We are working through a pseudo-spectral method[13], with Fourier expansion in the streamwise and spanwise directions, and Chebyshev expansion for the normal one. It is implemented on the structured non-staggered grid. It applies the $3/2$ rule de-aliasing technique. The temporal scheme is a fully-explicit second-order Adams-Bashforth time-integration method, and the computation code is based on MPI parallelization.

With these features, the models have been tested and validated for the homogeneous isotropic turbulence case[3], both in the decaying and forced simulations, showing good results compared

with classical Comte-Bellot & Corrsin experiment[14], for example. The channel flow [15] has also been tested and compared with the DNS of Moser et al.[16], yielding again proof of validity.

The general structure of the algorithm for the specific case of the boundary layer is a direct adaptation of the channel flow code, already successfully tested[13, 3]. It is based on the strong formulation of the Navier-Stokes equations with a Poisson - pressure correction term. The main changes are, as expected, on the initial velocity field, the boundary conditions, the algebraic scaling, and the Poisson solver.

The boundary conditions are the usually prescribed ones:

$$y = 0 \rightarrow u,v,w = 0 \tag{8}$$

$$y = \infty \rightarrow < u >= 1; v,w = 0 \tag{9}$$

3.1 Semi-infinite domain

One of the key issues of the boundary layer simulations is the semi-infinite domain and the scaling procedure over the normal direction, from $y\varepsilon[0,\infty)$. The Navier-Stokes must be reformulated in the presence of this scaling factor (sc):

$$\begin{aligned} \partial_t \overline{u} + C_{sc}(\overline{u},\overline{u}) + GT(\overline{u},\overline{U}) &= D_{sc}\overline{u} - \nabla_{sc} p - \nabla_{sc}\cdot\tau(\overline{u}); \\ \nabla_{sc}\cdot\overline{u} &= 0 \end{aligned} \tag{10}$$

For all the calculations, we have used the standard algebraic scaling[10]

$$\begin{aligned} y_\infty &= L\frac{1+y_1}{1-y_1} \qquad \text{smooth [0,}\infty\text{)} \\ \mathbf{sc}[\mathbf{y_1}] &\equiv \frac{dy_1}{dy_\infty} \qquad \text{smooth [2/L,0]} \end{aligned} \tag{11}$$

where y_∞ means the normal coordinate from 0 to ∞, and y_1 from -1 to 1 (the usual prescription for Chebyshev transforms), L is a parameter and $\mathbf{sc}[\mathbf{y_1}]$ means the scaling factor. The prescription of the L parameter is somewhat arbitrary: the value is barely related to the number of points in the normal direction[10]. We have fixed the value to $L = 2.5$.

For clarity, we show the change that the scaling produces in some of the terms of the Navier-Stokes equations. So, for the x or streamwise direction:

- The convective term:

$$u\frac{\partial u}{\partial x} + v\cdot\mathbf{sc}[\mathbf{y_1}]\frac{\partial u}{\partial y_1} + w\frac{\partial u}{\partial z} \tag{12}$$

- The diffusive term:

$$\nu\left(\frac{\partial^2 u}{\partial x^2} + \mathbf{sc}[\mathbf{y_1}]\frac{\partial}{\partial y_1}\left(\mathbf{sc}[\mathbf{y_1}]\frac{\partial u}{\partial y_1}\right) + \frac{\partial^2 u}{\partial z^2}\right) \tag{13}$$

- The Poisson equation:

$$\frac{\partial^2 P}{\partial x^2} + \mathbf{sc}[\mathbf{y_1}]\frac{\partial}{\partial y_1}\left(\mathbf{sc}[\mathbf{y_1}]\frac{\partial P}{\partial y_1}\right) + \frac{\partial^2 P}{\partial z^2} = \frac{\partial u}{\partial x} + \mathbf{sc}[\mathbf{y_1}]\frac{\partial v}{\partial y_1} + \frac{\partial w}{\partial z} \tag{14}$$

It also introduces spurious terms that must be removed.

- The S3PQR algorithm

$$\frac{\partial}{\partial x}(\nu_e[x,y,z]\frac{\partial u}{\partial x}) + \mathbf{sc}[\mathbf{y_1}]\frac{\partial}{\partial y_1}(\nu_e[x,y,z]\cdot\mathbf{sc}[\mathbf{y_1}]\frac{\partial u}{\partial y_1}) + \frac{\partial}{\partial z}(\nu_e[x,y,z]\frac{\partial u}{\partial z}) \tag{15}$$

The scaling factor enters into the ν_e calculation via the Δ subgrid characteristic length and the several invariants involved.

4. Model Deployment and First Results

For all the current computations, the grid size of the domain is $Nx = 32$, $Ny = 64$, and $Nz = 32$ points, where x, y, and z, are the streamwise, wall-normal, and spanwise directions. The Reynolds number is fixed along the simulation to $Re_{\delta^*} = 1000$, where δ^* is the displacement thickness.

4.1 Boundary layer

First, we deal with the free boundary layer cases without the turbine model. As we have said before, the structure of the algorithm for a boundary layer is based on the method proposed by Spalart and Leonard (1987) [11].

To compare the LES models and the Spalart and Leonard (1987) [11] results, we can list three main parameters: u_τ as the friction velocity, H as the ratio of the displacement thickness to the momentum thickness, and κ as the Von Kármán constant (see Table 1, where SL stands for the reference DNS values).

Table 1: boundary layer characteristic parameters calculated for each model. First column results from reference. Grid size for all the other cases: 32x64x32. Vr. as Vreman's model

Case:	SL	No mod.	Vr.	WALE	PQ1	PR1	QR1	PQ2	PR2	QR2
u_τ	**0.049**	0.049	0.050	0.046	0.048	0.050	0.049	0.046	0.049	0.048
H	**1.52**	1.61	1.51	1.54	1.58	1.54	1.57	1.57	1.53	1.57
κ	**0.39**	0.35	0.47	0.47	0.35	0.44	0.35	0.42	0.39	0.32

The Smagorinsky method did not yield meaningful results with the current algorithm (incorrect near-wall behavior). The rest of the LES models give reasonable results. All of the S3PQR cases present comparable values, with PR2 standing as nearly the best in the global analysis. As an example of the performance of this model, we plot the velocity profile and the root mean square of the velocities (Figure 1). The main differences between the models can be seen in plotting the derivative of the velocity profile y^+du^+/dy^+ (see Figure 2). As Spalart recalls in his work [12], the logarithmic layer corresponds to the minimum, and the value of κ is thus determined, despite the noise due to the lack of resolution. Moreover, the values of the maxima can be directly compared with that of Spalart.

We can also plot the rms u^+ values for all of them (Figure 3) yielding no further discrimination between the models, but as a demonstration of their similar performance.

Then we can confidently say that S3PQR models capture the general trend. Besides, the PR2 model values are within the range of the expected ones. Moreover, PR2 also performs

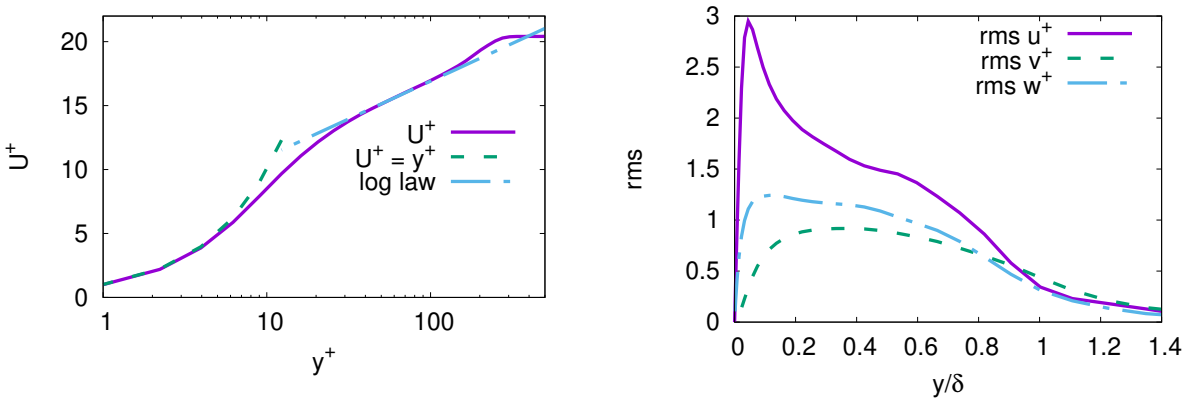

Figure 1: Case PR2, present results. Left: normalized average streamwise velocity profile, U^+; log law; $U^+ = y^+$. Right: rms u^+; rms v^+; rms w^+; δ is the boundary layer thickness

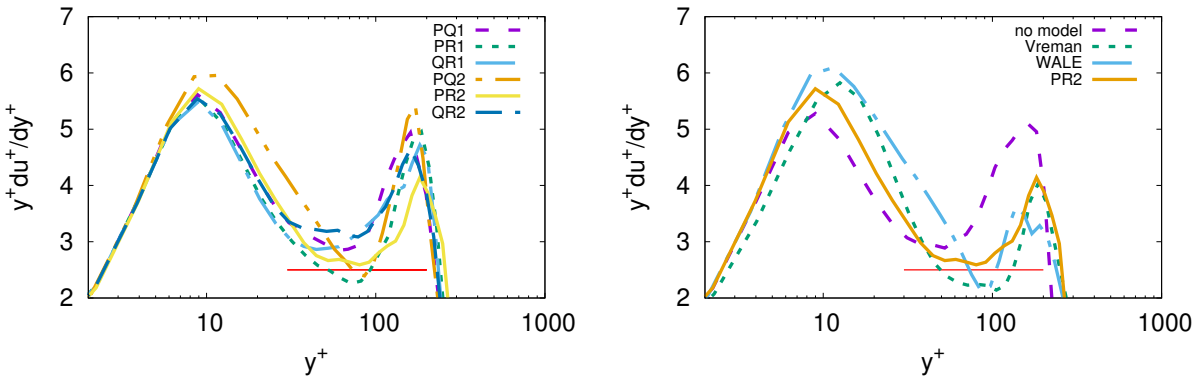

Figure 2: y^+du^+/dy^+ vs y^+. Left: S3PQR models. Right: comparison with other LES models. The horizontal line marks the point(s) where the log law would be with $\kappa = 0.4$

better than Vreman, WALE, or no-model algorithms. Thus so far we have obtained reliable results with low computational effort for the free boundary layer.

4.2 Wind farm

We will follow the model stated by Calaf et al [17]. They rely on the concept of a fully developed boundary layer to use periodic conditions, whereas we work with the assumptions of Spalart as we have seen.

They also develop the concept of a disk actuator for every wind turbine. The force of the turbine (per unit mass), in the streamwise direction, at a given grid point i, j, k, is given by

$$F(i,j,k) = -\frac{1}{2} C_T' \langle \overline{u}^T \rangle_d^2 \frac{\gamma_{j,k}}{\Delta x}$$

where C_T' is a thrust coefficient, $\langle \overline{u}^T \rangle_d^2$ is the disk averaged local velocity, $\gamma_{j,k}$ is the fraction area overlap of the disk and Δx is the distance between turbines.

This disk actuator model can be straightforwardly applied to our algorithm. We will compute our wind farm with the same number and array geometry of the turbines that a specific case

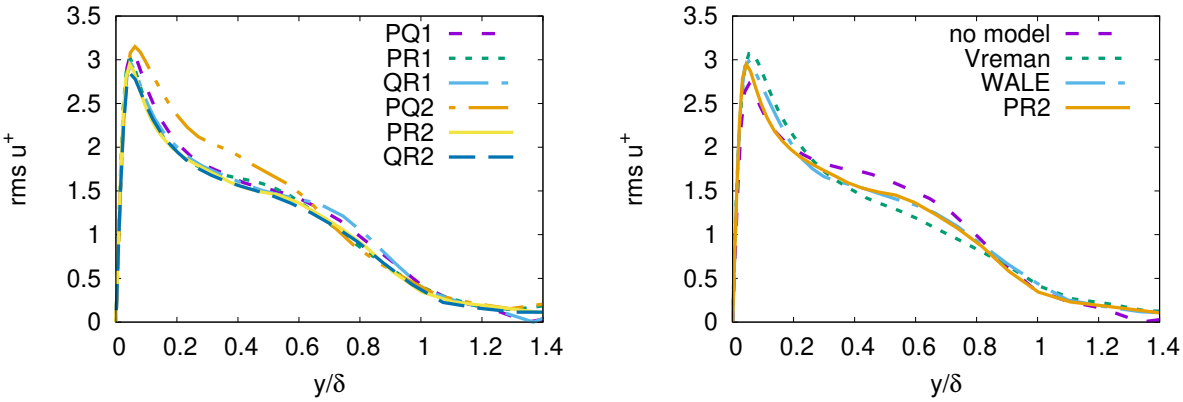

Figure 3: rms u^+. Left: S3PQR models. Right: comparison with other LES models

of the reference: 24 disk actuators evenly distributed in four rows and six columns (see Figure 4). Later on, we will change this geometrical configuration.

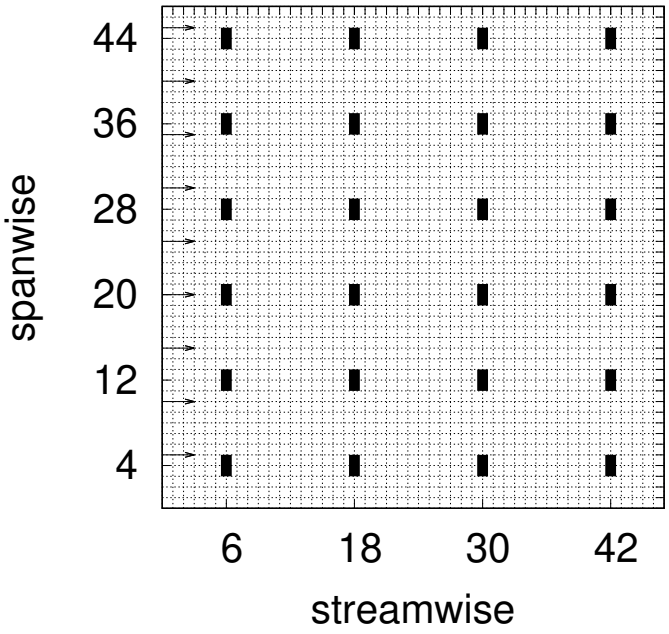

Figure 4: Geometrical layout of the disk actuators. Ranges expressed in terms of the 48x48 de-aliasing 3/2 rule domain. Arrows pointing as a sketch of the velocity at the top

However, there are differences in all other configuration parameters such as Reynolds' number, energy supply, and wall boundary conditions. Moreover, the adaptation of Spalart's boundary layer method to that of the wind farm poses some challenges. First of all, the growing terms of Spalart that supply energy to the system rely on the existence of one single log law and its transition to a velocity defect law. The main parameter is friction velocity. In the case of the wind farm, we expect two log laws [17] with two defined friction velocities. The solution adopted in this case is simply an average between the two friction velocities, so the error for the

growing terms is, at least, reasonably bounded.

Therefore, a comparison can be based only on the horizontal profile behavior and magnitude order of values at this time. In Figure 5, on the left, we show the results for the velocity profile with PR2. On the right, some energy terms values. In Figure 6, the general behavior of the velocity profile for all of them.

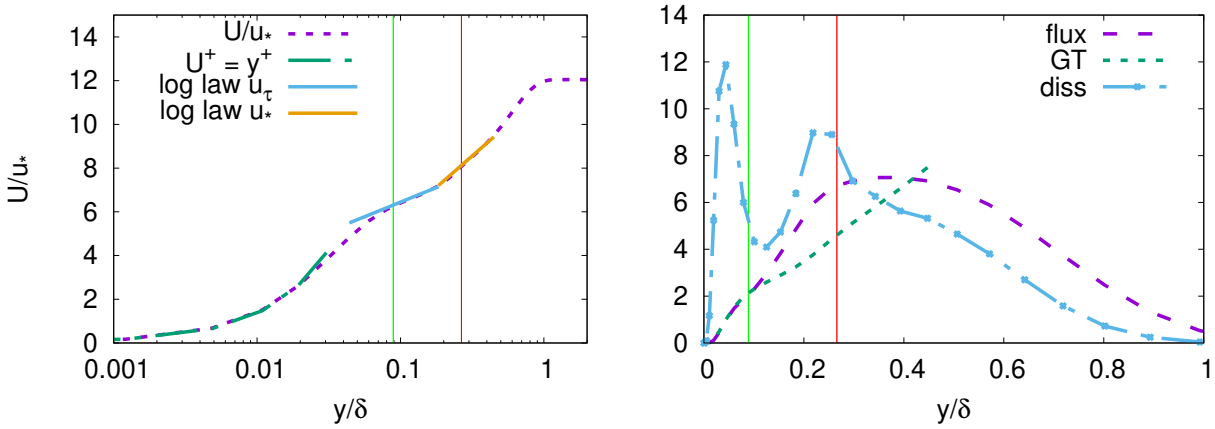

Figure 5: Model PR2 as an example. Left: average streamwise velocity. The green vertical line is the position of the bottom of the turbine hub. The red line is the top. Note the law of the wall and the two log laws. Right: Normalized mean kinetic energy contributions: **flux**, $\delta\Phi = - < uv > U/u_*^3$; **GT**, normalized growing terms; **diss**, $- < uv > \partial_y U/(u_*^3/\delta)$

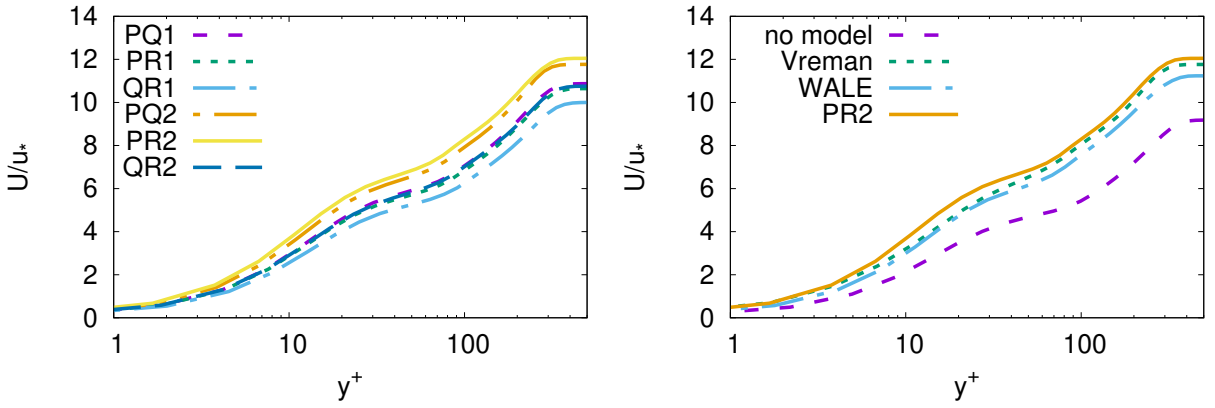

Figure 6: Velocity profiles. Left: S3PQR. Right: other LES models. The no-model discrepancy could be due to a miscalculated u^* because no second log law is apparent

Some of the several quantities that may be of interest are listed in Table 2. The meaning of the terms is as follows:

$z0_{Hi}/zH$, as the ratio of the effective roughness above the turbine hub and the height of the turbines' center (it should be written $y0_{Hi}/yH$ but we used the reference nomenclature);

u_τ, the usual friction velocity at the wall;

u_*, the computed friction velocity above the hub; P, the time and horizontally averaged power extracted for every turbine;

W_t, the time, horizontally, and vertically (along the hub) averaged power;
$\delta\Phi$, the vertical flux of kinetic energy;
Finally, the term EB (for energy budget) is the balance between all the energy contribution terms. For a perfect match, it should be 100% (the reference achieves 98%).

All the magnitudes are of the same order as reference. From the column of $P/\delta\Phi$, it is observed that it also reproduces the observed behavior that the wind turbines, in a fully developed boundary layer regime, extract kinetic energy using vertical fluxes.

Table 2: some computed useful quantities of a wind farm simulation. Grid size:32x64x32

MODEL	$z0_{Hi}/zH$	u_τ	u_*	u_τ/u_*	$P/\delta\Phi$	$W_t/\delta\Phi$	EB
no model	0.160	0.051	0.109	0.47	0.68	0.81	94%
Vreman	0.072	0.056	0.085	0.66	0.67	0.78	94%
WALE	0.082	0.050	0.089	0.56	0.79	0.90	94%
PQ1	0.096	0.052	0.092	0.57	0.75	0.86	96%
PR1	0.105	0.052	0.094	0.55	0.74	0.85	95%
QR1	0.123	0.052	0.100	0.52	0.73	0.84	95%
PQ2	0.074	0.052	0.085	0.61	0.75	0.86	95%
PR2	0.065	0.052	0.083	0.63	0.77	0.88	97%
QR2	0.098	0.052	0.093	0.56	0.74	0.86	95%

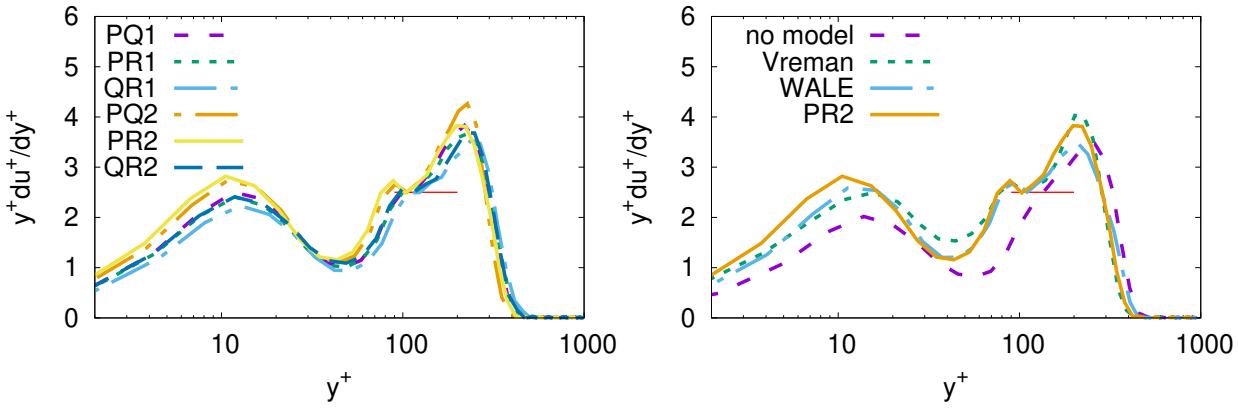

Figure 7: y^+du^+/dy^+. All the values normalized by u_*; left: S3PQR models. Right: other LES models. Note the presence of one or two minima corresponding to the log laws. The horizontal line shows the expected second log law with, by definition, $\kappa = 0.4$ Note too, that in cases where it is present, it appears approximately in the same position

Recall that as shown in [17], we can expect two well-defined log laws along the vertical velocity profile, represented as two minima in the y^+du^+/dy^+ vs y^+ plot. In the present algorithm and configuration, QR1 and no-model fail to yield these two log laws, while PQ1 and PR1, barely do. Despite this, for them, we have calculated the values as if there were a log law in the same approximate position as it appears in the other models (see Figure 7). The remaining ones fulfill this condition, as can be seen in the same figure.

The lack of this second log law could be due again to noise (the derivative is more sensitive to it), low resolution, or intrinsic behavior of the models. The question remains open to future work.

4.3 Wind turbines' positions

As a practical application of these S3PQR models, we have selected the PR2 algorithm to analyze the power extraction for several configuration patterns of the wind farm turbines' positions. These patterns are ordered (4 rows 6 columns used in all the previous work, Figure 4), and six more configurations that we call: "alternated", "diagonal", two "curved", and two "disordered" ones. The distance between rows, Δx, has been kept the same as the original calculation. The geometrical patterns can be seen in Figure 8.

PATTERN	$P/\delta\Phi$	P/u^{*3}
ordered	0.77	3.24
alternated	0.80	3.31
diagonal	0.80	3.10
curved#1	0.76	2.87
curved#2	0.77	2.86
disordered#1	0.79	3.05
disordered#2	0.76	3.05

Table 3: PR2 model. Position energy-related quantities of a wind farm simulation. All normalized by u^* of the ordered geometry.

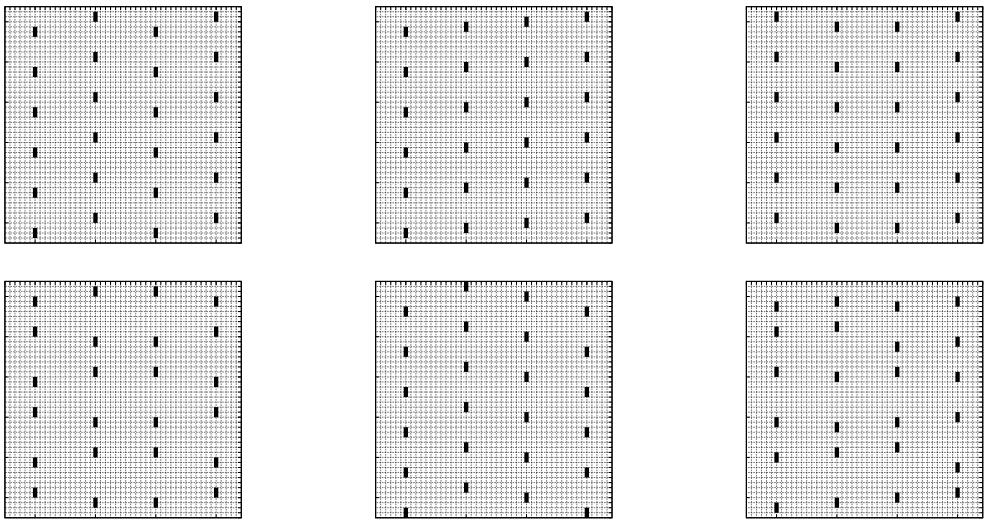

Figure 8: Positions' patterns. From the top left, in order: alternated, diagonal, curved#1, curved#2, disordered#1, disordered#2. Same interpretation as Figure 4

The results are shown in Table 3, with no striking differences between them. It is as expected, because the energy extracted by the turbines in a fully developed boundary layer comes from vertical fluxes, minimizing the dependency on the horizontal pattern geometry.

5. Conclusions

Without benchmark values for all these particular cases of wind farm configurations, it may be bold to assess which model gives better results or whether S3PQR algorithms are better than other LES models because all of them (except the no-model) are in the same range of values. But for most of them, the general behavior matches that of reference, either on the boundary layer or the wind farm cases.

Therefore, what we can confidently say at this moment is that at least the S3PQR type 2 algorithms are well-suited to be included in every LES test for a broad range of cases, starting from homogeneous isotropic turbulence and channel flow to free boundary layer and wind farm simulations.

References

1. F. Nicoud, H. B. Toda, O. Cabrit, S. Bose, and J. Lee, "Using singular values to build a subgrid-scale model for large eddy simulations," *Physics of Fluids*, vol. 23, no. 8, p. 085106, 2011.
2. C. Meneveau and J. Katz, "Scale-Invariance and Turbulence Models for Large-Eddy Simulation," *Annual Review of Fluid Mechanics*, vol. 32(1), p. 1–32, 2000.
3. F. X. Trias, D. Folch, A. Gorobets, and A. Oliva, "Building proper invariants for eddy-viscosity subgrid-scale models," *Physics of Fluids*, vol. 27, no. 6, p. 065103, 2015.
4. J. Smagorinsky, "General Circulation Experiments with the Primitive Equations," *Monthly Weather Review*, vol. 91, pp. 99–164, 1963.
5. A. W. Vreman, "An eddy-viscosity subgrid-scale model for turbulent shear flow: Algebraic theory and applications," *Physics of Fluids*, vol. 16, no. 10, pp. 3670–3681, 2004.
6. F. Nicoud and F. Ducros, "Subgrid-scale stress modelling based on the square of the velocity gradient tensor," *Flow, Turbulence and Combustion*, vol. 62, no. 3, pp. 183–200, 1999.
7. R. Verstappen, "When does eddy viscosity damp subfilter scales sufficiently?," *Journal of Scientific Computing*, vol. 49, no. 1, pp. 94–110, 2011.
8. R. A. Clark, J. H. Ferziger, and W. C. Reynolds, "Evaluation of subgrid-scale models using an accurately simulated turbulent flow," *Journal Fluid Mechanics*, vol. 91, pp. 1–16, 1979.
9. D. R. Chapman and G. D. Kuhn, "The limiting behaviour of turbulence near a wall," *Journal of Fluid Mechanics*, vol. 170, pp. 265–292, 1986.
10. J. P. Boyd, *Chebyshev and Fourier Spectral Methods*. Dover Publications, Inc., 2001.
11. P. Spalart and A. Leonard, *Direct Numerical Simulation of Equilibrium Turbulent Boundary Layers*. Berlin: Springer-Verlag, 1987.
12. P. Spalart, "Direct simulation of a turbulent boundary layer up to $R_\theta = 1410$," *Journal of Fluid Mechanics*, vol. 187, pp. 61–98, 1988.
13. F. X. Trias, D. Folch, A. Gorobets, and A. Oliva, "Spectrally-consistent regularization of Navier-Stokes equations," *Journal of Scientific Computing*, vol. 79, pp. 992–1014, 2019.
14. G. Comte-Bellot and S. Corrsin, "Simple Eulerian time correlation of full- and narrow-band velocity signals in grid-generated, isotropic turbulence," *Journal of Fluid Mechanics*, vol. 48, pp. 273–337, 1971.
15. F. X. Trias, A. Gorobets, and A. Oliva, "A simple approach to discretize the viscous term with spatially varying (eddy-)viscosity," *Journal of Computational Physics*, vol. 253, pp. 405–417, 2013.

16. R. D. Moser, J. Kim, and N. N. Mansour, "Direct numerical simulation of turbulent channel flow up to $Re_\tau = 590$," *Physics of Fluids*, vol. 11, pp. 943–945, 1999.
17. M. Calaf, C. Meneveau, and J. Meyers, "Large eddy simulation study of fully developed wind-turbine array boundary layers," *Physics of Fluids*, vol. 22, p. 015110, 2010.